Subwavelength far-field ultrasound drug-delivery

Article *in* Applied Physics Letters · November 2016

DOI: 10.1063/1.4967009

Subwavelength far-field ultrasound drug-delivery

Authors: Vincent Hingot, Marine Bézagu, Claudia Errico, Yann Desailly, Romain Bocheux, Mickael Tanter, Olivier Couture

Affiliations : Institut Langevin, CNRS, INSERM, ESPCI Paris, PSL Research University, 17 rue Moreau, 75012, Paris, France.

Keywords : Ultrasound, ultrafast, delivery, super-resolution, localization, acoustic droplet vaporization

Abstract:

The theoretical diffraction-limit of resolution for ultrasound imaging has recently been bypassed in-vitro and in-vivo. However, in the context of ultrasound therapy, the precision of therapeutic beams remains bound to the half-wavelength limit. By combining acoustic vaporization of composite droplets and rapid ultrasound monitoring, we demonstrate that ultrasound drug-delivery can be restricted to a subwavelength zone. Moreover, two release zones closer than wavelength/4 can be distinguished both optically and through ultrafast ultrasound localization microscopy. This proof-of-concept let us envision the possibility to treat specific tissue more precisely without compromising on the penetration depth of the ultrasound wave.

Main text

Ultrasound waves can perform both diagnostic and therapeutic procedures. Ultrasound imaging highlights, in real-time, anatomical and physiological information in soft-tissue. Additionally, higher intensity ultrasound can thermally treat tumors [1]. It can also be used to induce the passage of drugs in cells [2] or brain tissue [3] or even to release the drugs themselves using ultrasound-sensitive injectable agents [4].

Because of its wave nature, ultrasound resolution is limited by diffraction both in the imaging and therapeutic field. In the medical frequency spectrum, wavelengths range from 100 µm to 1mm, which confines precision to the sub-millimetric range in the far-field. Higher frequencies implies increased attenuation leading to a fundamental compromise between resolution and penetration. This fact imposes the use of a specific piezoelectric array for each application.

We recently introduced a technique [5] that bypasses the diffraction limit in ultrasound imaging, achieving resolution of about 8 µm at 12 mm depth for the vascular structure of the rat brain [6]. This method was inspired by optical localization techniques such as FPALM [7].

However, as of today, therapeutic ultrasound remains limited by the diffraction limit. This implies that small lesions can be detected, but cannot be treated without affecting the surrounding tissues, which can be fragile, such as nerves, arteries or brain tissue. Moreover, the ultrasound therapeutic frequency cannot significantly be reduced to treat deeper or transcranial structures, without directly affecting the accuracy of the therapy.

This manuscript was accepted by Appl. Phys. Lett. Click here to see the version of record.

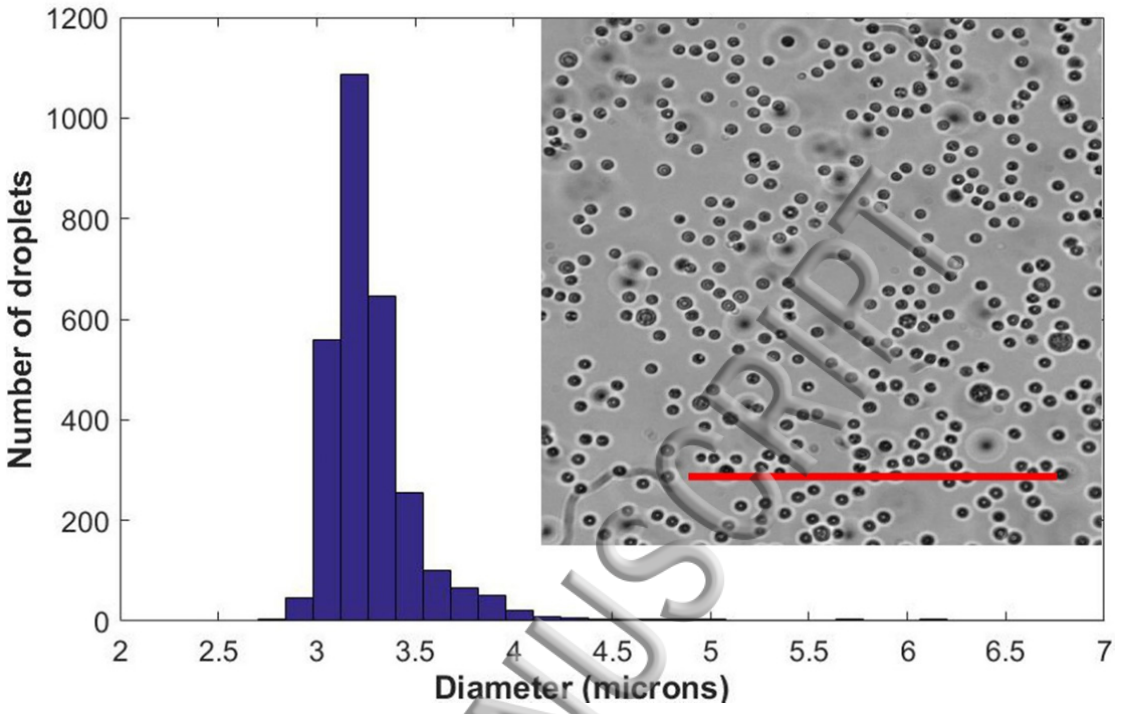

Figure 1: Distribution of the diameter of the composite droplets (mean = 3.3 μm, standard deviation = 0.3 μm). In overlay, microscope image of the composite droplets (scale bar = 100 μm)

In this paper, we propose an approach to attain subwavelength precision in a form of ultrasonic therapy, namely targeted drug-delivery. To achieve this goal, we exploit the interaction between ultrasound and ultrasound-sensitive agents characterized by a very sharp release pressure threshold [8, 9]. These microdroplets were introduced for localized drug-delivery using acoustic vaporization [10]. They are formed as a double emulsion (water in perfluorohexane (PFH) in water) where the PFH phase acts both as a barrier between the inner phase and the outer phase, but also as a vaporizable matrix that converts into a gas with an appropriate drop in pressure initiated by an ultrasound wave. As they are produced with a microfluidic system, they are monodisperse making their conversion pressure threshold abrupt. Moreover, the conversion into gas is readily detectable by an ultrasound scanner as it leads to a rapid increase in echogenicity, within milliseconds.

We propose to use this sharp pressure threshold and constant monitoring to convert droplets exclusively within a subwavelength area by intercepting only a small fraction of the ultrasound focal spot. By gradually increasing the ultrasound pressure, we can attain a point where only a fraction of these droplets are induced in the core vicinity of the focal spot.

Specifically, the first step to fabricate the composite droplets is to sonicate for 40s a mixture of perfluorohexane (PFH) and fluorinated surfactant (3 % w/v) with an aqueous solution of fluorescein in saline (2 % w/v). The resulting water-in-PFH nanoparticles are between 200-300 nm in diameter. This solution is then injected in a highly parallelized microfluidic droplet generator based on a terrace geometry (128 channels, 4.2 μm width and 0.6 μm height, with

a terrace length of 7.30 µm, **(adapted from [11])**. The external fluid is water with Pluronic-68 surfactant (2 % w/v). As shown in figure 1, the resulting composite droplets, water-PFH-water, are monodisperse with an average diameter of 3.3 µm and polydispersity of 9%. As described before, the content of the droplets is released by an acoustic pulse with sufficient pressure, which allow visualization of the free fluorescein.

Approximatively 10 million composite droplets are injected in a cellular culture plate placed horizontally in a water-bath for acoustical coupling (figure 2). The plate is observed through a macroscope (Leica, MZ10F) with a 8X magnification and pictures are taken with an SLR camera (Canon EOS70D). This plate is also placed above a 128-elements linear array used at 5 MHz pulse frequency, leading to a 300 µm wavelength in water. The array is piloted by a programmable ultrasound scanner capable of ultrafast imaging capabilities, able of emitting arbitrary pulses over the 128 channels and recording their echoes to achieve frame rates of several thousand frames per second. It is used to generate focused pulses for ultrasound-induced delivery with increasing pressures between 2 and 5.2 MPa peak-negative pressure (4 µs duration). For monitoring, delivery pulses are followed by 200 plane-wave images (13 kHz frame rate), creating sequences 30 ms long in total (410 emissions). Between sequences, the focused pulses are incrementally increased by a minimum of 80 kPa until droplet release is observed acoustically.

The release monitoring is performed by subtracting ultrasound echoes following the focused release pulse with those obtained prior to it. When perfluorohexane liquid is converted into gas, the resulting bubbles increases rapidly the echogenicity from that specific spot, a change easily detected through differential ultrafast imaging as nothing else is changing within 100 µs. This monitoring is exploited to stop the increment in pressure at the level where ultrasound delivery is detected.

Of primary importance is the focal spot profile of the focused pulses shown in figure 2b. Indeed, the release zone is determined by the intersection between the spatial distribution of acoustic pressure and the acoustic threshold for the release of the droplets. As the array is linear, focusing can only be controlled in the lateral direction which displays a thinner beam profile. In the elevation direction, focusing is performed by a fixed lens that cannot be modified. Here, the focal spot is calculated with Field-II [12] for a linear array with 0.2 mm pitch, 8 mm transducer elevation height, a 45 mm focus and a 30 mm fixed elevation focus at 5 MHz. This simulation provides a theoretical prediction of the delivery spot.

This manuscript was accepted by Appl. Phys. Lett. Click here to see the version of record.

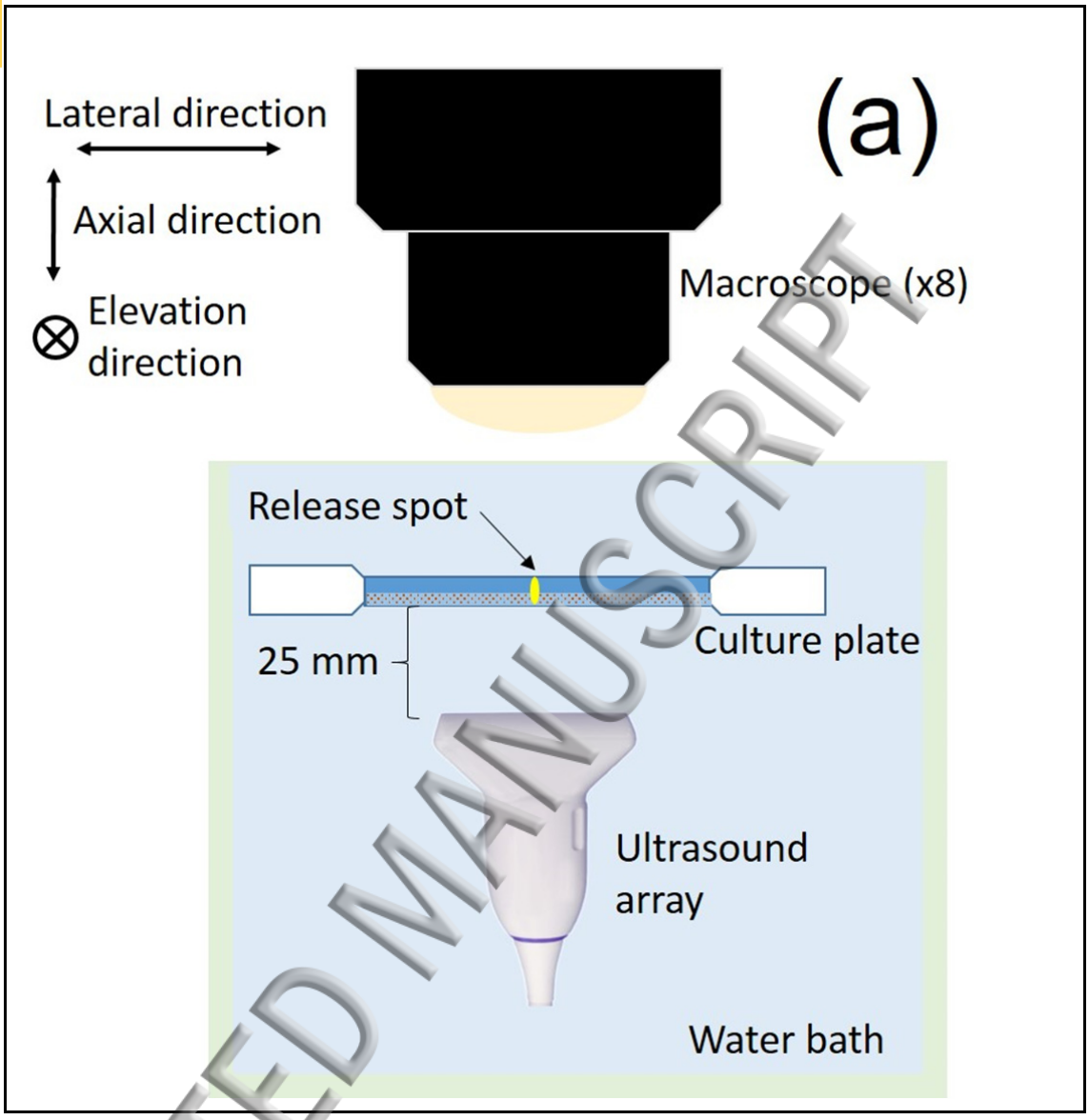

This manuscript was accepted by Appl. Phys. Lett. Click here to see the version of record.

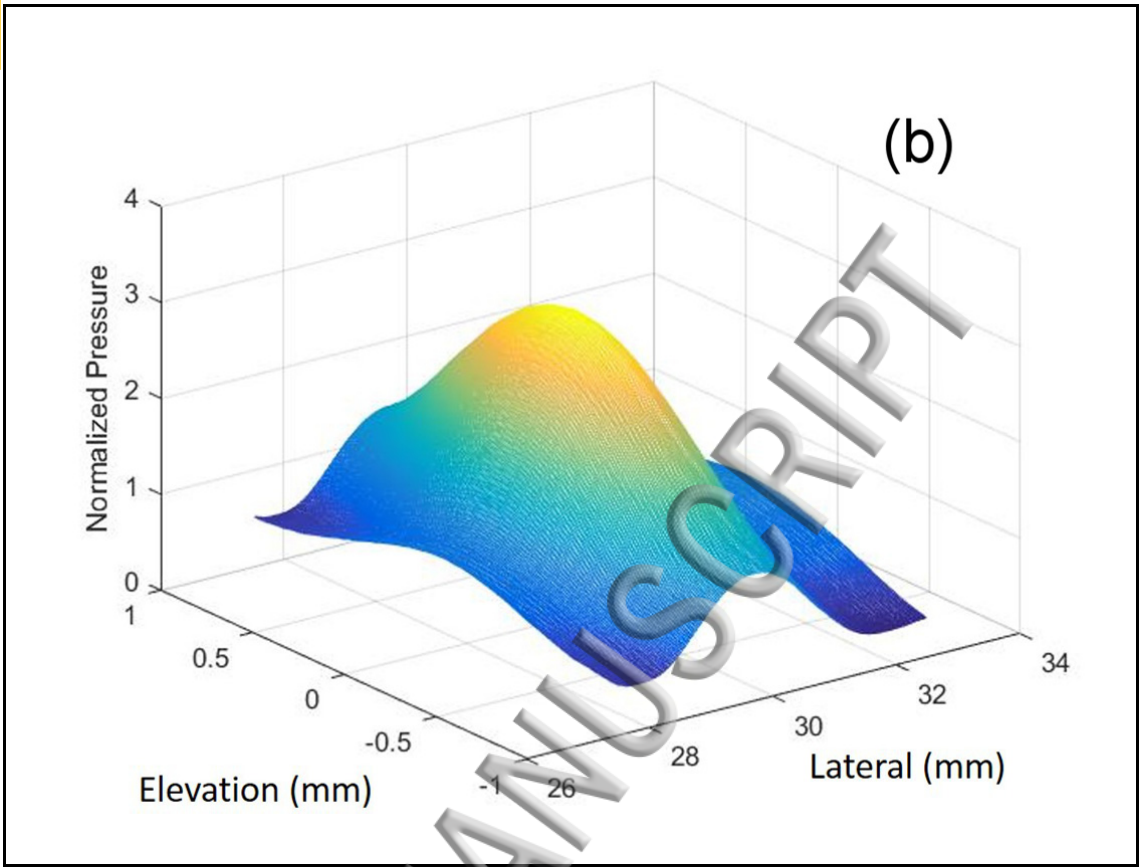

Figure 2: a) Setup used for the in-vitro demonstration of subwavelength delivery. The culture plate is placed between a macroscope and an ultrasonic linear array piloted by a programmable ultrafast ultrasound scanner. b) Simulated profile of the peak pressure around the focus of the ultrasonic array. Elevation and Lateral directions are shown in (a).

The first experiment consisted in observing the release zone following the emission of one focused pulse at a precise location in the culture plate, just above the acoustic threshold for droplets' conversion. Figures 3abcd show the increasing size of the release spot with increasing peak acoustic pressure. As a larger zone undergo acoustic pressure beyond the threshold, the total number of converted droplets increases. For the lowest pressures, the release spot is significantly smaller than the wavelength. In the lateral direction, the release spot can be as small as 70 µm, which is smaller than a fourth of the wavelength. As the pressure is increased, it can reach one wavelength in size. Since electronic focusing cannot be performed in the elevation direction of the linear array, the resolution is degraded in this direction, creating anisotropic spots.

This manuscript was accepted by Appl. Phys. Lett. Click here to see the version of record.

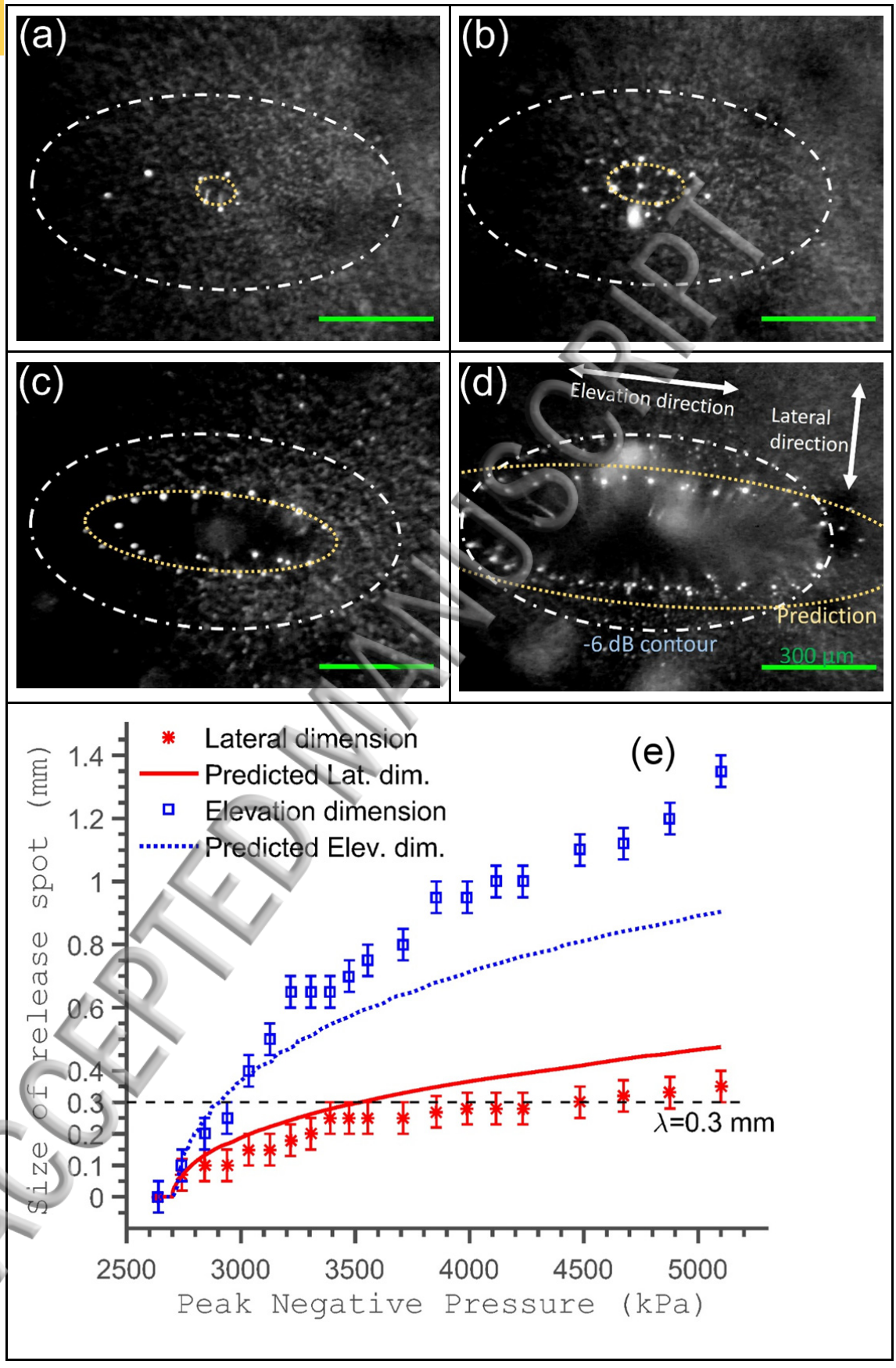

Figure 3: Delivery spot in the culture plate following a focused ultrasound pulse at various peak negative pressure a) 2.6 MPa b) 2.7 MPa c) 3.2 MPa d) 5.1 MPa (scale bar = 300 µm, dotted blue line represents the -6dB maximum pressure contour and the dotted yellow line is activation pressure threshold contour). The droplets are depleted in the release spot and, following radiation pressure, the resulting large bubbles or droplets are collected on its circumference. The yellow ellipse correspond to the release spot predicted from the activation pressure threshold and the white ellipse correspond to the full-width at half maximum of the focal spot profile. e) Experimental spot size, in the lateral and elevation direction, increasing with the peak pressure.

The general behavior of the spot size can be simply predicted by simulating the focal spot profile of the array, with Field-II [12], and determining the surface intercepted by the threshold (figure 2b). The relationship for the lateral and elevation direction, along with the subwavelength release spots, are rightly predicted for the lowest pressures. However, the spot size at larger pressures is not appropriately predicted. This could be due to the fact that the pressure field is not modelled appropriately. Measurement could also be contaminated by radiation pressure, which can displace droplets from a wider zone than the area affected by ultrasonic release. Faster cameras could discriminate droplets that are vaporized from those that are simply pushed away.

The second experiment consisted in delivering two spots much closer than the wavelength and observing the gap with the optical macroscope and ultrasound localization microscopy. In figure 4abc, two release spots are created within the same delivery sequence lasting 30 ms. In this case, their gap is programmed with electronic delays to be 70 µm in the lateral direction. 15 ms after the first release, the second spot is indeed created at the defined distance. However, due to the fixed lens in the elevation direction, the focal spot is wider and lacks uniformity. To better define the distance between the deliveries, profiles of the release spots were created by integrating the optical intensity in the elevation direction (figure 4e). The wavelength/4.2 gap between the two spot is better defined, even though a modification in the optical intensity remains from the first delivery during the second acquisition.

If the two release spot are clearly distinct optically, it should also be important to distinguish them acoustically. In this case, ultrasound localization microscopy can be exploited. Indeed, each release is followed by 200 plane-wave ultrafast images obtained within 15 ms. The two release spots obtained after acoustic beamforming of the difference in echo before and after the ultrasonic delivery is shown in figure 5a and 5b. Each of these 200 images can be interpolated and their maximum can be found with a high precision since the release zone should be smaller than the wavelength. By plotting the position of the center of each image, the real distance between the two focal spot can be evaluated with a precision of wavelength/3.

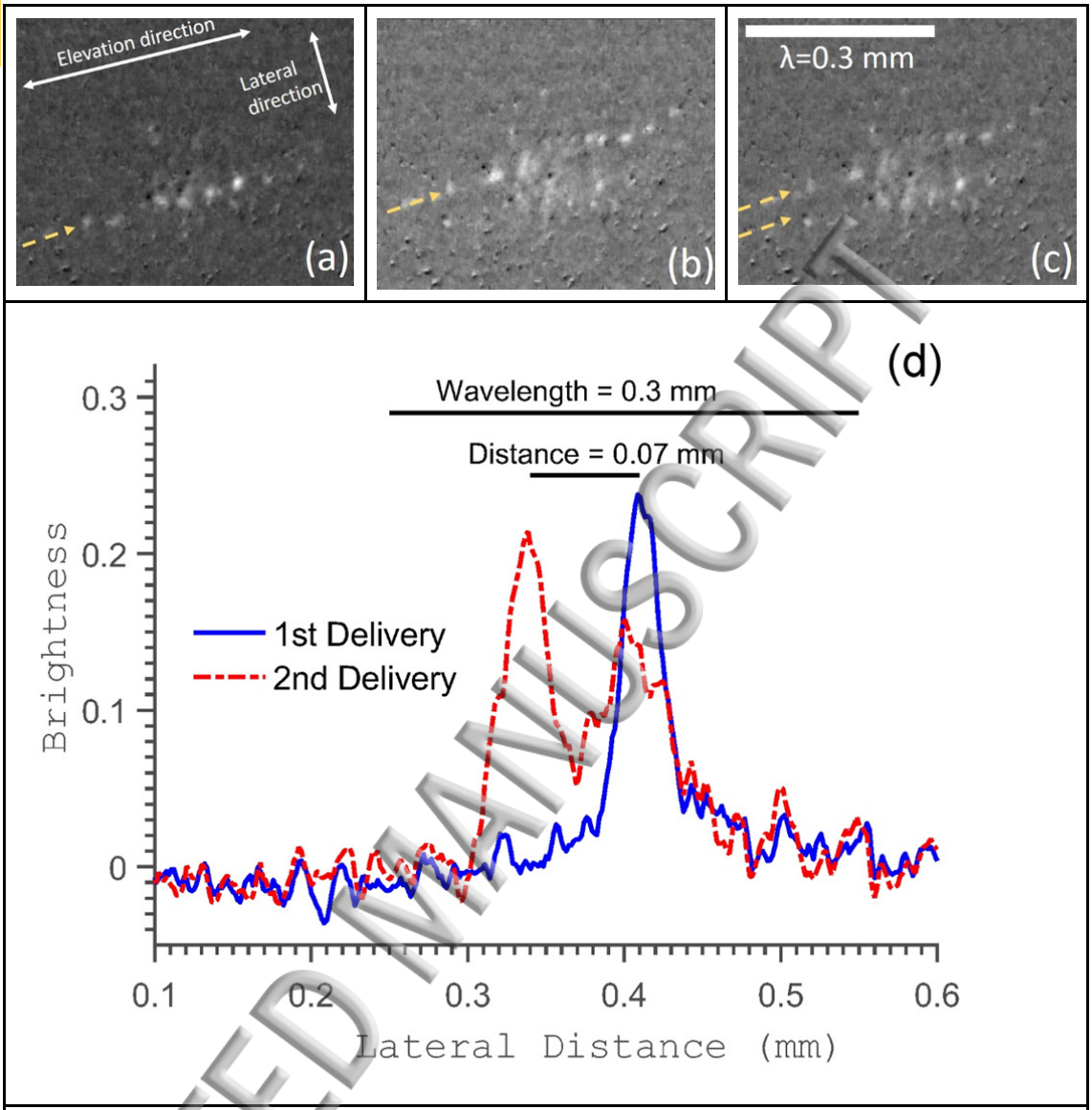

Figure 4: Two delivery spots distant of wavelength/4.2 observed optically. a) First delivery b) Second delivery 15 ms later. c) Superposition of the two to display the gap d) Profile of the integrated intensity in the elevation direction showing a clear distinction between the two delivery spot.

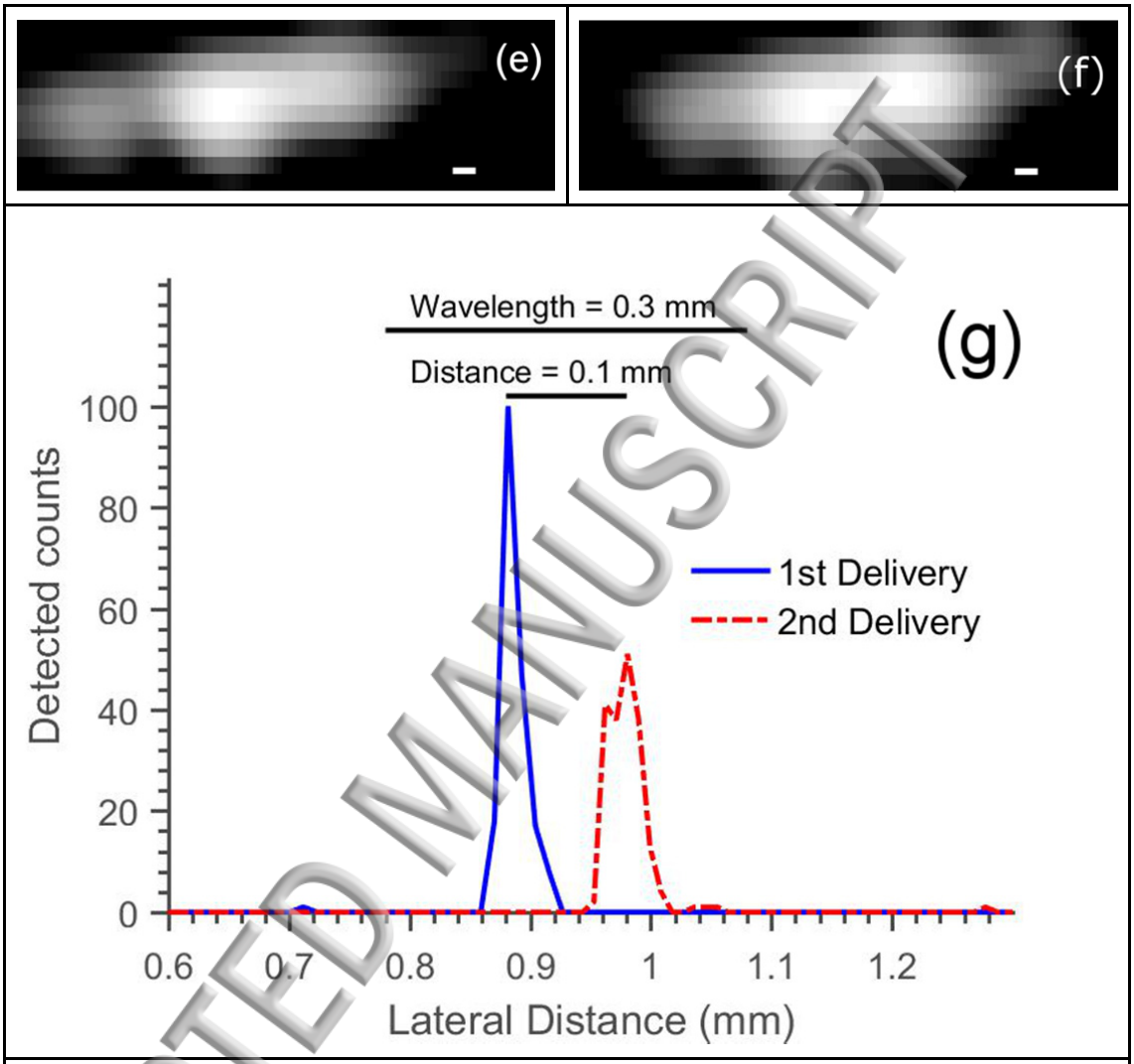

Figure 5: Two delivery spots distant of wavelength/3 observed acoustically. a) Differential plane-wave image 70 us after the first delivery (scale bar = 100 □m) b) Second delivery spot c) Histogram of the position of the interpolated maximum peak of the ultrasound echo showing the appropriate gap between the two releases.

In this study, we wished to demonstrate that an ultrasonic therapy, in this case triggered delivery, can be performed with a precision better than a half-wavelength. It can be paralleled to the recently introduced ultrasound localization microscopy, even though it uses a different approach to bypass the diffraction-limit. For the therapeutic part, we rely on a threshold effect, which can be compared to nonlinear phenomena exploited in optics for improved resolution [13]. Spot size and separation of 70 µm (or wavelength/4.2) could be observed optically. Subwavelength monitoring based on ultrasound localization microscopy could also be demonstrated for wavelength/3 separation. However, droplet release could

This manuscript was accepted by Appl. Phys. Lett. Click here to see the version of record.

not reach comparable resolution than its imaging counterpart, which shows microvascular structures, wavelength/12 in size.

The abrupt threshold of the droplet conversion is a necessary condition for subwavelength delivery and would be difficult to apply for thermal-based therapy. Nevertheless, other than composite droplets, various cavitation-based phenomena could be candidates for subwavelength ultrasonic therapy. Histotripsy, for instance, has already shown very precise boundaries in their therapeutic zone [14]. Compression-only microbubbles [15] or phase-shift agents [16,17] could also be exploited for their threshold-like onset.

The local momentary conversion of the droplet must be detectable for practical implementation. In-vivo conditions implies variabilities in tissue structures which make such that the local peak pressure cannot be predicted theoretically or numerically. Reaching the threshold must be measured in real-time for the process to be terminated just above the conversion threshold. Since it implies the formation of gas bubbles, ultrafast ultrasound [18] monitoring seems to be particularly appropriate for this task. For this, ultrasound release must have a sufficient signal-to-noise ratio to be detected. Moreover, the shape of the super-resolved delivery spot can be affected by aberrations caused by heterogeneities in the acoustic properties of the propagating medium. In general, a better estimate of the pressure field at the focal spot could be obtained with a 3D raster scan of a calibrated hydrophone in the region of the focus. However, it would not take tissue aberrations into account and would remain approximate.

The applicability of the method also implies that a large lesion can be treated with a precise border. Considering that the droplet release is obtained with pulses lasting 4 µs and that the following monitoring lasts 15 ms, a single breathhold (10s) would allow hundreds of subwavelength delivery spots to be generated.

Despite these limitations, we could envision a precise ultrasound-based theranostic device, where the wavelength does not imply a compromise between resolution and penetration. Target tissue could be highlighted with ultrasound localization microscopy and then treated with a precision in the tens of microns, providing an accurate tool to address small or infiltrating lesions.

Acknowledgments

This work was supported principally by Agence Nationale de la Recherche, within the project ANR MUSLI. It was also supported by LABEX WIFI (Laboratory of Excellence ANR-10-LABX-24) within the French Program 'Investments for the Future' under reference ANR-10-IDEX-0001-02 PSL*.

References

[1] ter Haar, G. Progress in biophysics and molecular biology, 93(1), p.111 (2007).

[2] Bouakaz, A., Zeghimi, A. and Doinikov, A.A., Sonoporation: Concept and Mechanisms. In Therapeutic Ultrasound. Springer International Publishing, p.175 (2016).

[3] Burgess, A. and Hynynen, K., Microbubble-Assisted Ultrasound for Drug Delivery in the Brain and Central Nervous System. In Therapeutic Ultrasound Springer International Publishing, p. 293 (2016).

[4] Couture, O., Foley J., Kassel N.F., Larrat B. and Aubry J.-F. Transl Cancer Res 3(5), p. 494 (2014).

[5] Couture, O., Besson, B., Montaldo, G., Fink, M., & Tanter, M. Microbubble ultrasound super-localization imaging (MUSLI). IEEE Ultrasonics Symposium, p. 1285-1287 (2011).

[6] Errico, C., Pierre, J., Pezet, S., Desailly, Y., Lenkei, Z., Couture, O. and Tanter, M. Nature, 527(7579), p. 499 (2015).

[7] Betzig, E., Patterson, G.H., Sougrat, R., Lindwasser, O.W., Olenych, S., Bonifacino, J.S., Davidson, M.W., Lippincott-Schwartz, J. and Hess, H.F., Science, 313(5793), p.1642 (2006).

[8] Couture, O., Faivre, M., Pannacci, N., Babataheri, A., Servois, V., Tabeling, P. and Tanter, M. Medical physics,38(2), p 1116 (2011)

[9] Couture, O., Urban, A., Bretagne, A., Martinez, L., Tanter, M. and Tabeling, P. Medical physics, 39(8), p 5229 (2012).

[10] Kripfgans, O.D., Fowlkes, J.B., Miller, D.L., Eldevik, O.P. and Carson, P.L. Ultrasound in medicine & biology, 26(7), p.1177 (2000).

[11] Cohen C, Giles R, Sergeyeva V, Mittal N, Tabeling P, Zerrouki D, Baudry J, Bibette J, Bremond N. Microfluid Nanofluid (2014).

[12] Jensen, J.A. and Svendsen, N.B. IEEE transactions on ultrasonics, ferroelectrics, and frequency control, 39(2), p.262 (1992).

[13] Gustafsson, M.G. Proceedings of the National Academy of Sciences of the United States of America, 102(37), p.13081 (2005).

[14] Roberts, W.W., Hall, T.L., Ives, K., Wolf, J.S., Fowlkes, J.B. and Cain, C.A. The Journal of urology,175(2), p.734 (2006).

[15] Emmer, M., Van Wamel, A., Goertz, D.E. and De Jong, N. Ultrasound in medicine & biology, 33(6), pp.941-949 (2007).

[16] Kawabata, K.I., Yoshizawa, A., Asami, R., Azuma, T., Yoshikawa, H., Watanabe, H., Sasaki, K., Hirata, K. and Umemura, S.I. IEEE Ultrasonics Symposium, p. 517 (2006).

[17] Sheeran, P.S., Luois, S.H., Mullin, L.B., Matsunaga, T.O. and Dayton, P.A.. Biomaterials, 33(11), p.3262 (2012).

[18] Tanter, M. and Fink, M. IEEE transactions on ultrasonics, ferroelectrics, and frequency control,61(1), p.102 (2014).

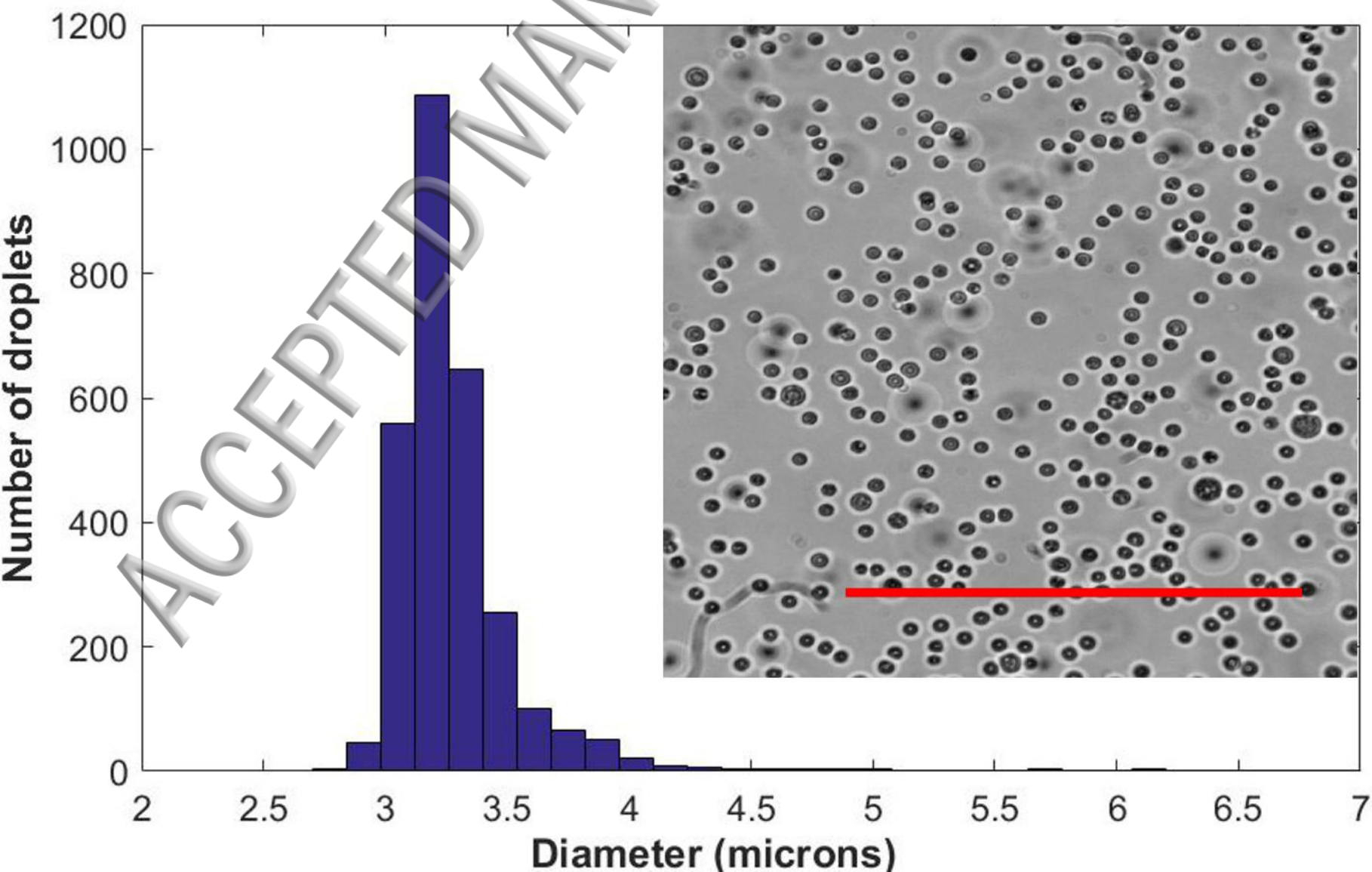

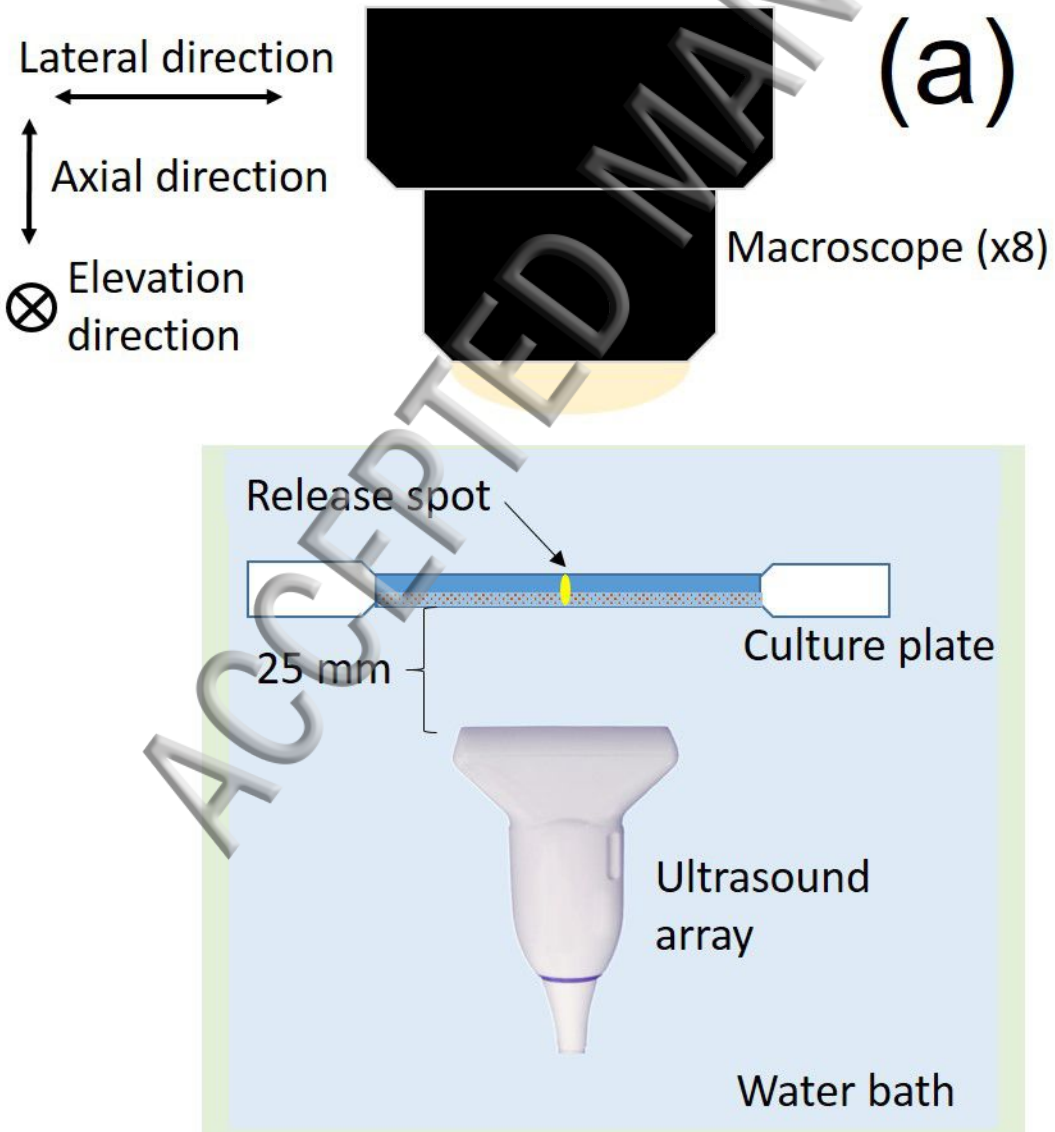

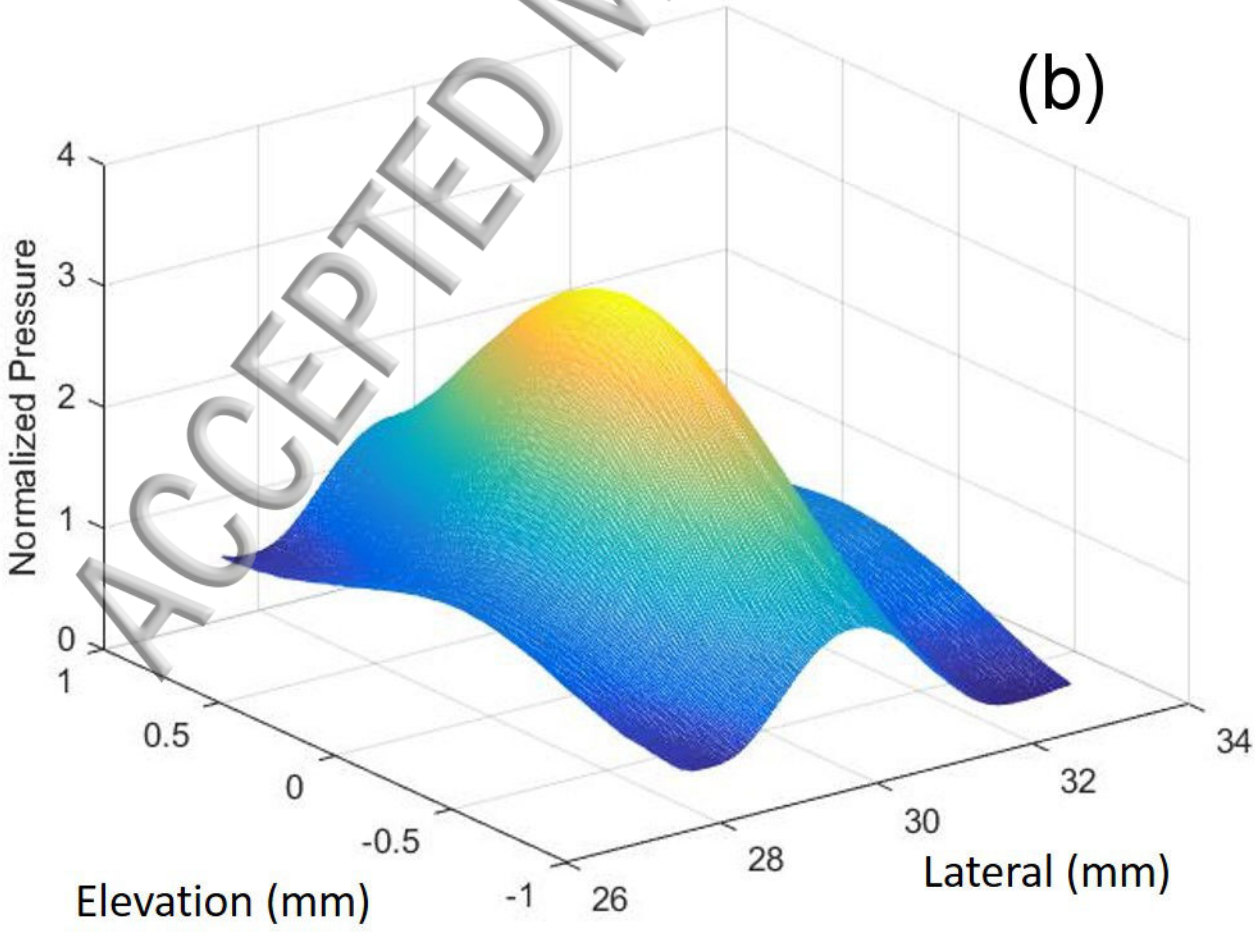
(b)
Normalized Pressure
4
3
2
1
0
1
0.5
0
-0.5
-1
Elevation (mm)
26
28
30
32
34
Lateral (mm)

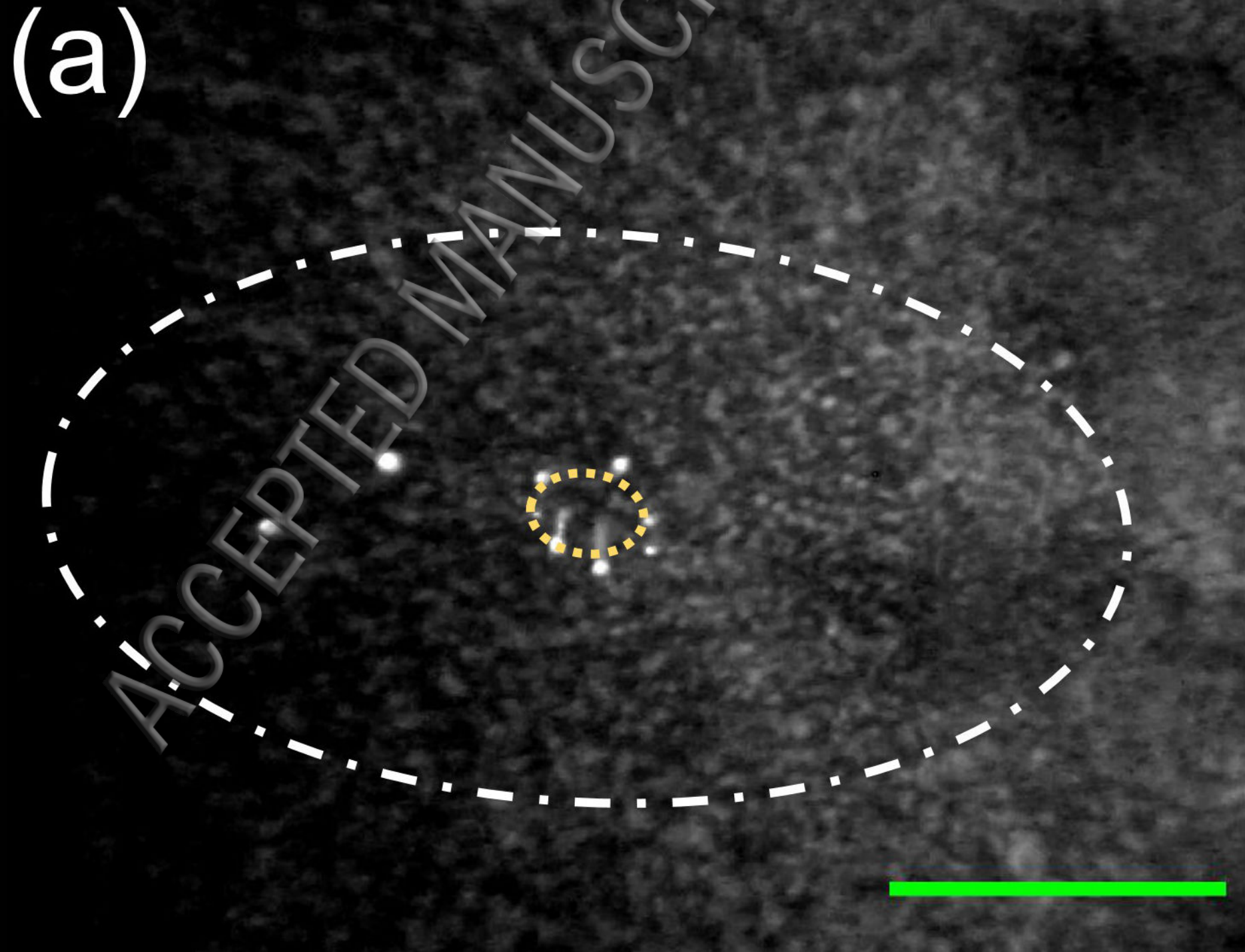

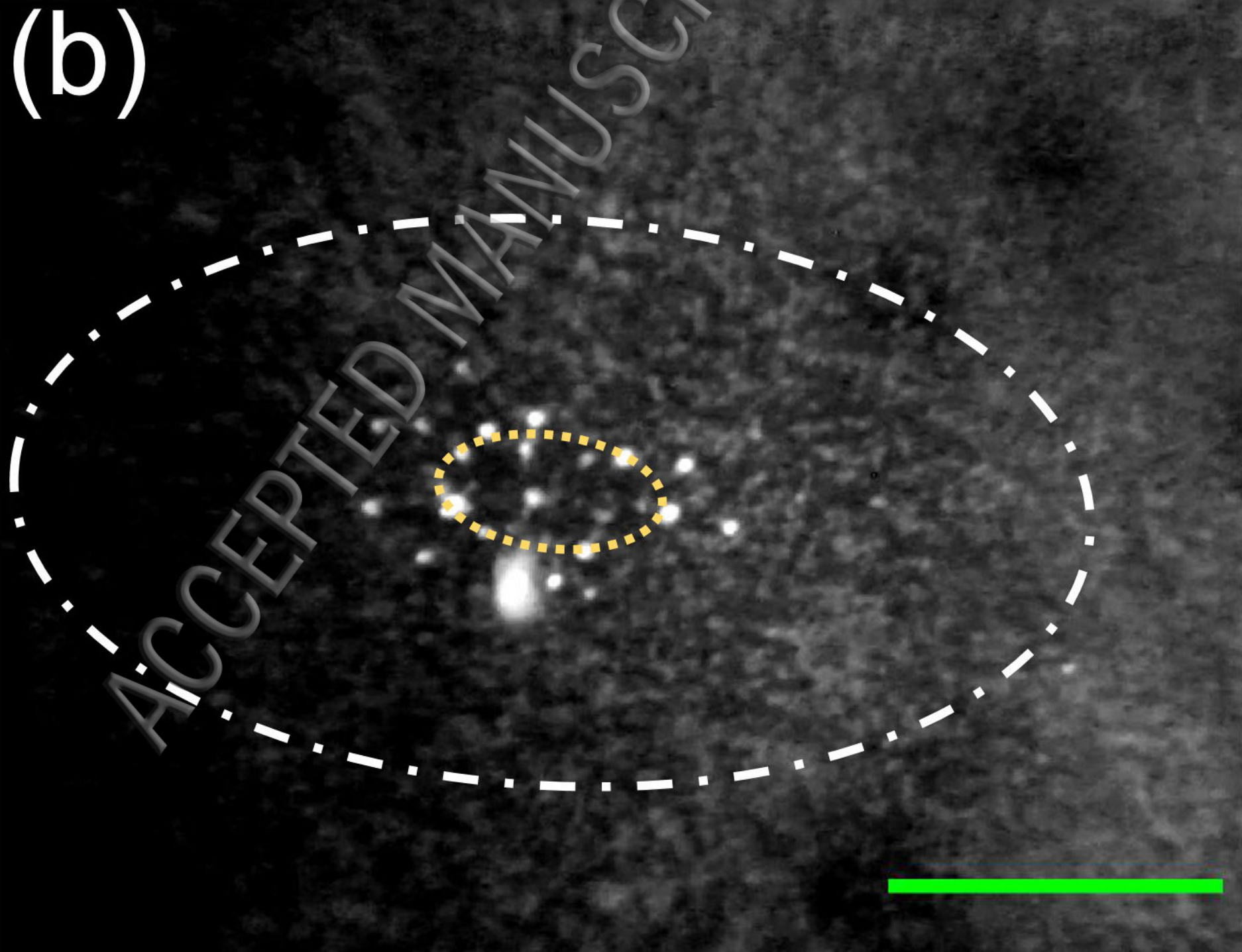

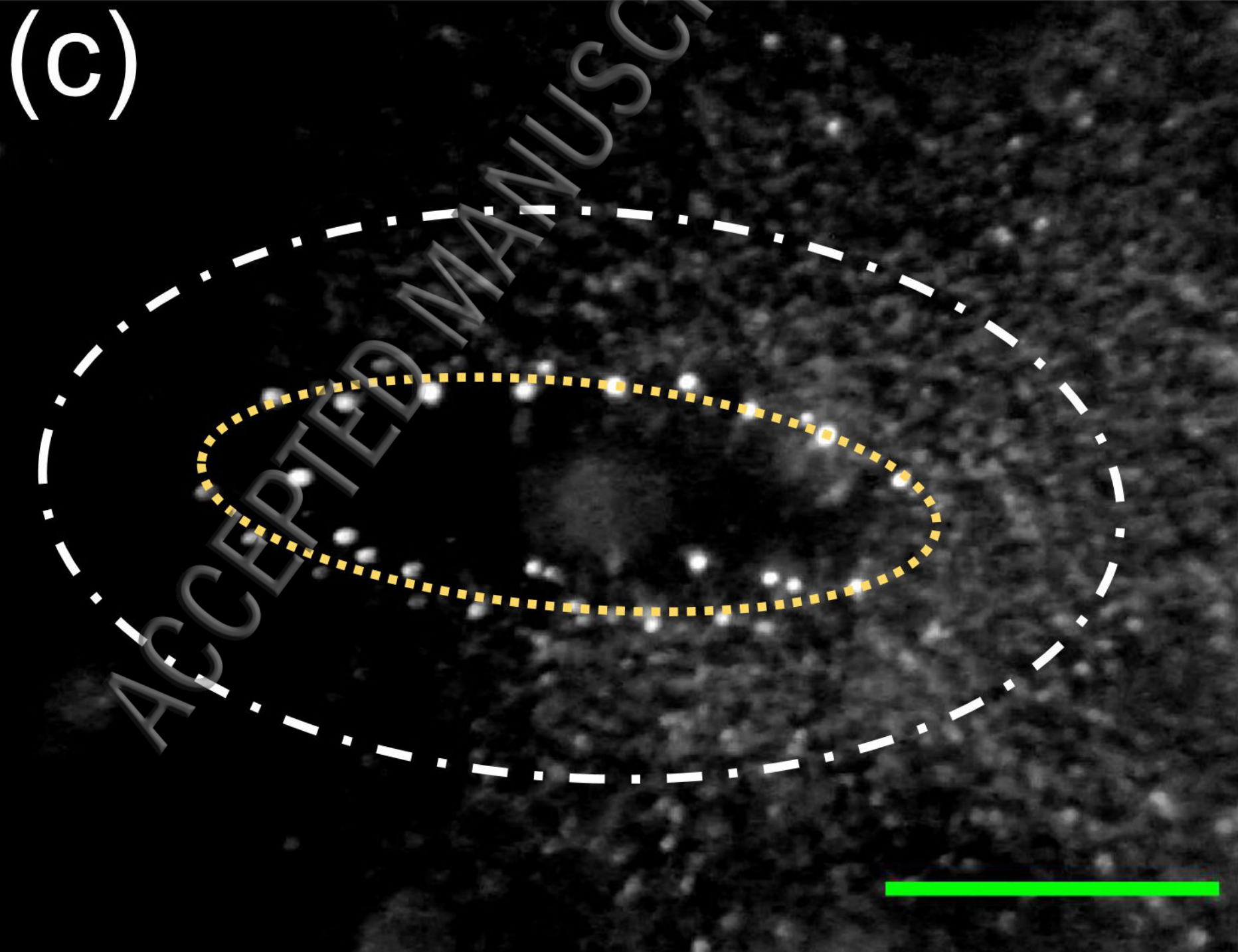

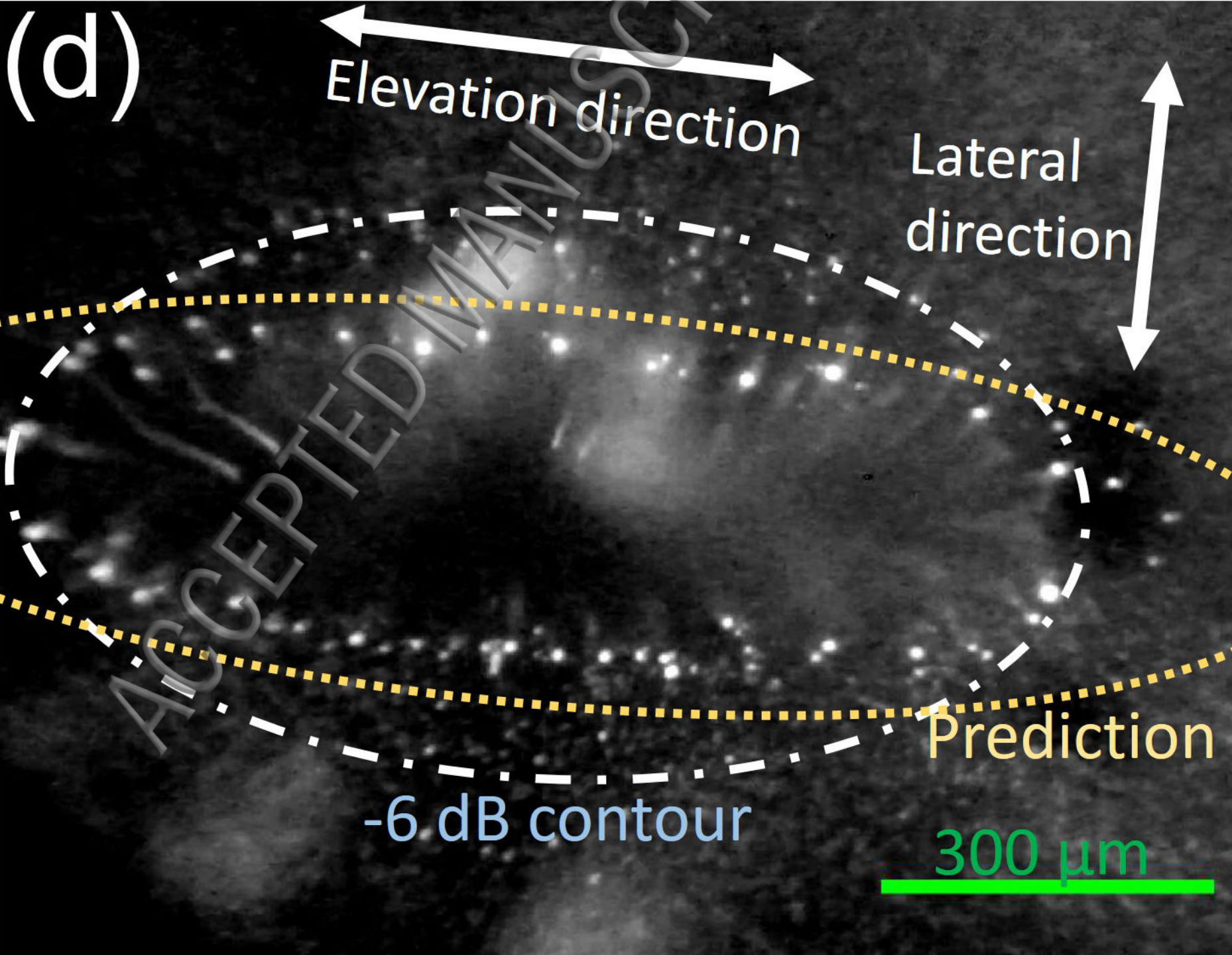

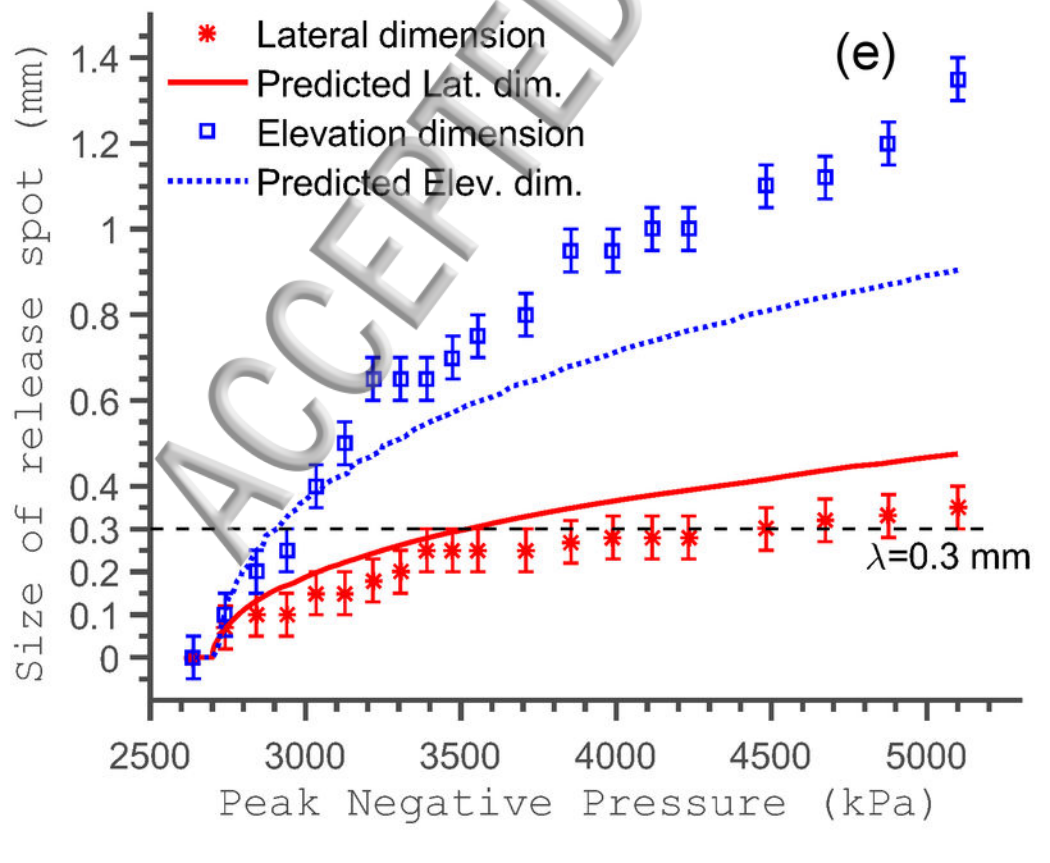
Lateral dimension
Predicted Lat. dim.
Elevation dimension
Predicted Elev. dim.
(e)
ACCEPTED
λ=0.3 mm
Size of release spot (mm)
Peak Negative Pressure (kPa)
0
0.1
0.2
0.3
0.4
0.6
0.8
1
1.2
1.4
2500
3000
3500
4000
4500
5000

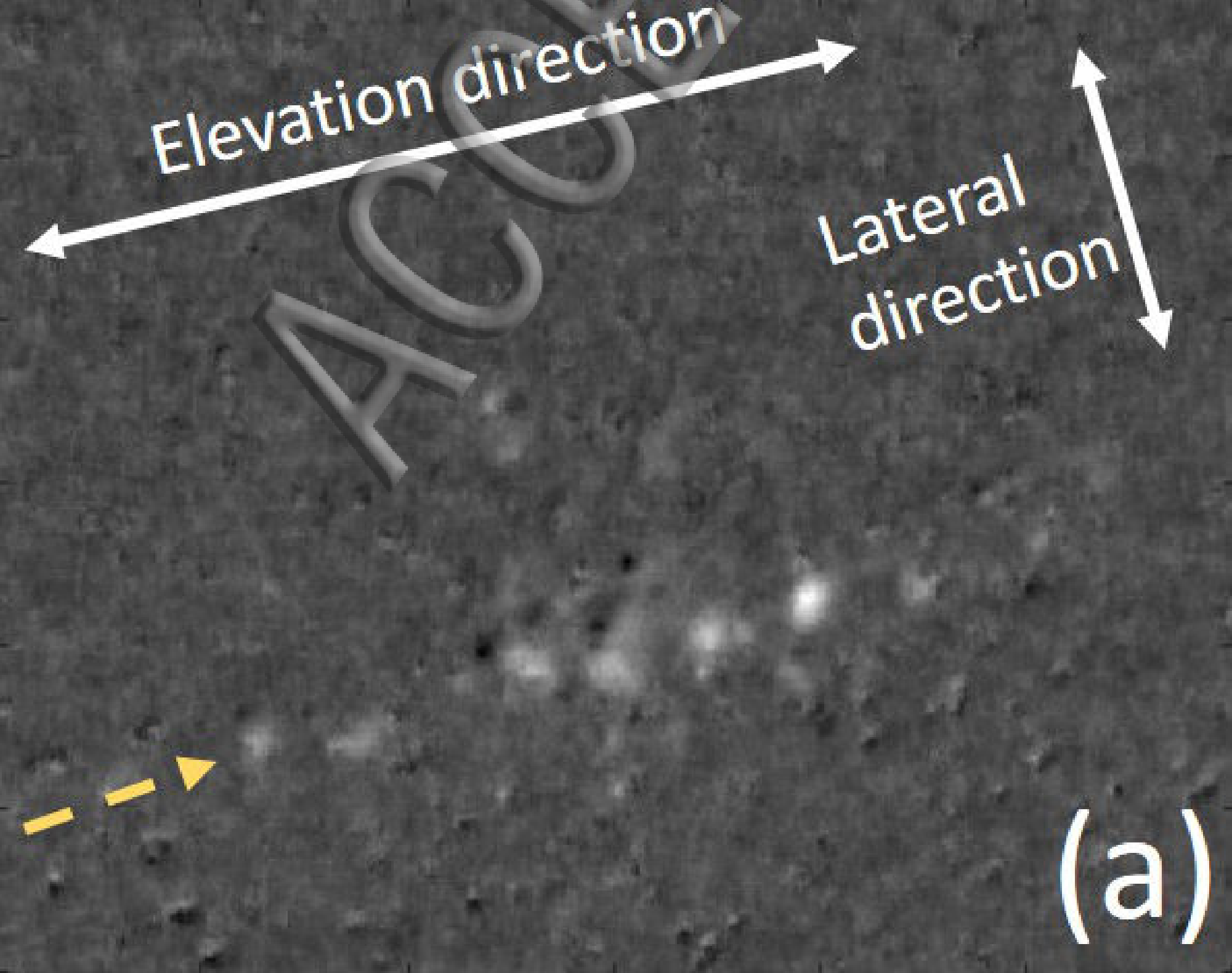
Elevation direction
Lateral direction
(a)


(b)

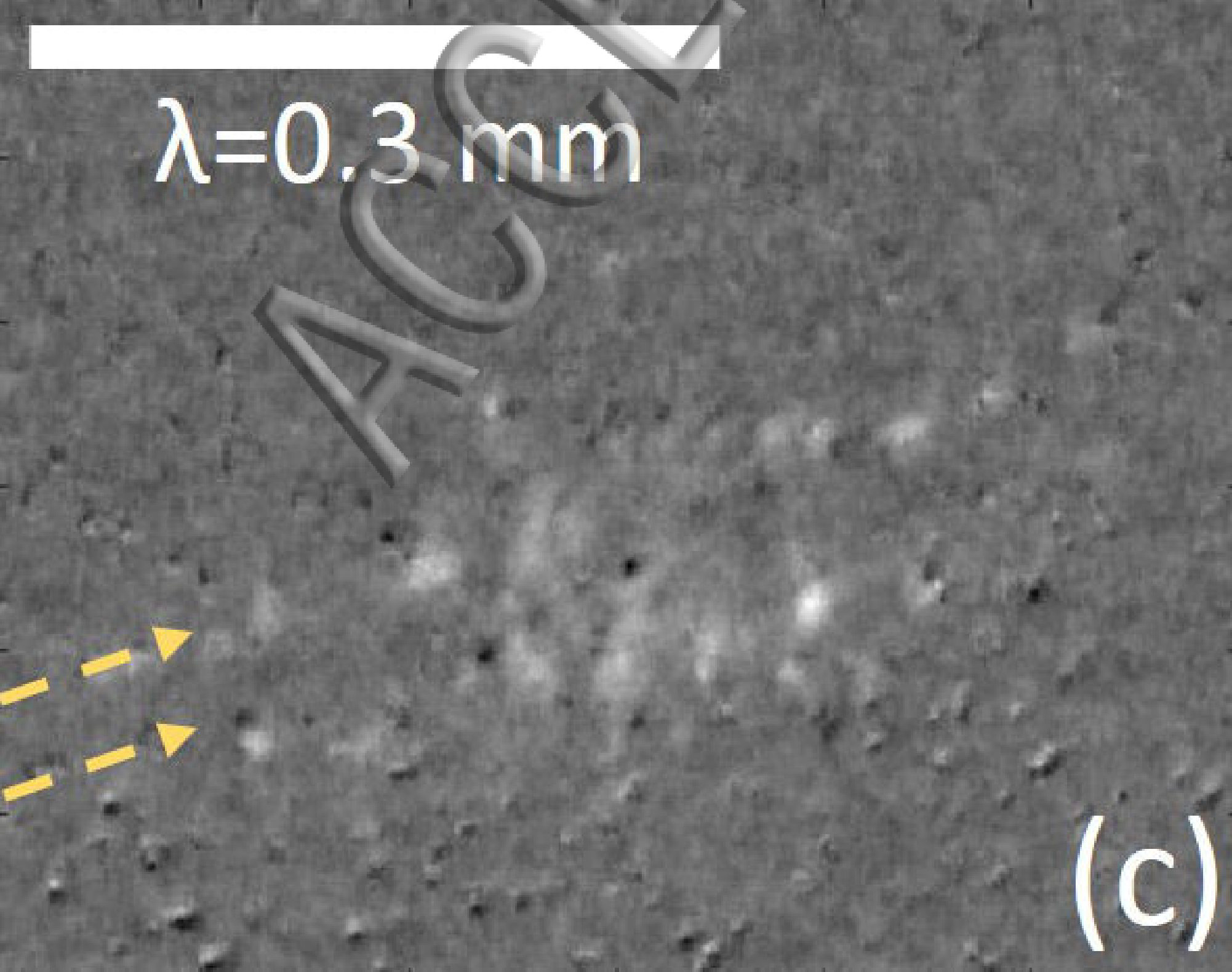
λ=0.3 mm
(c)

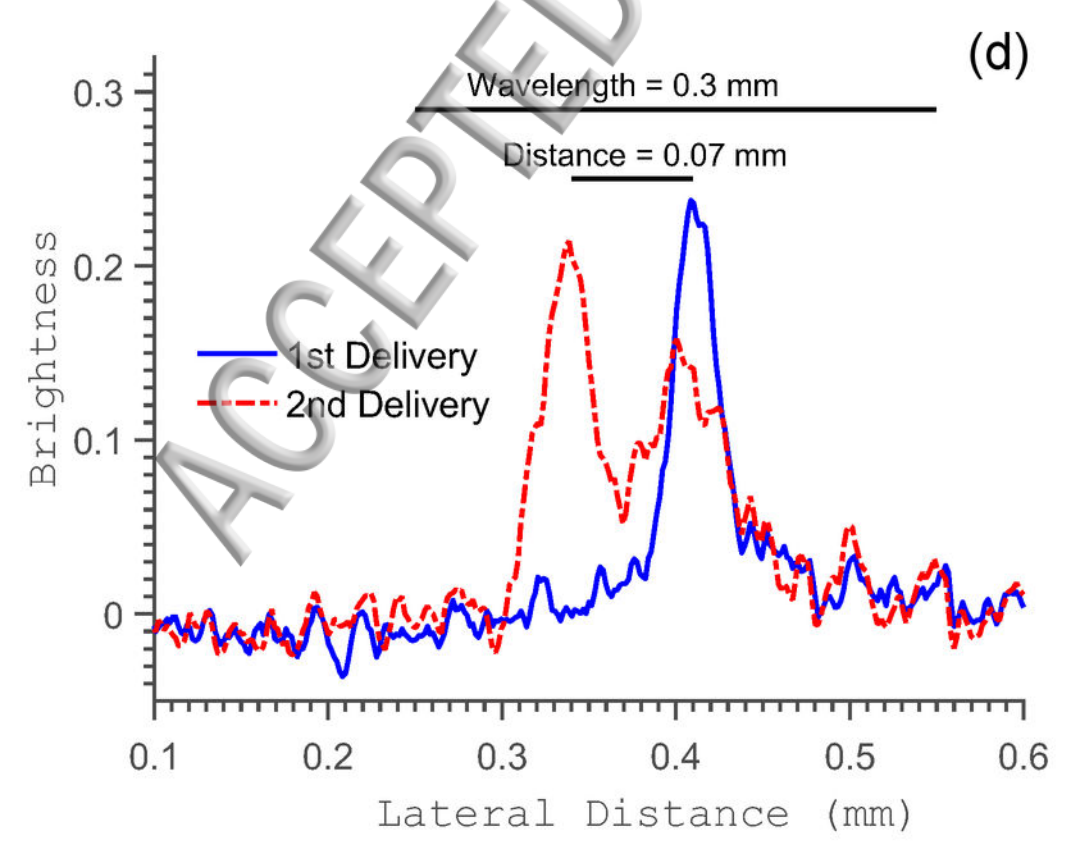
(d)
Wavelength = 0.3 mm
Distance = 0.07 mm
1st Delivery
2nd Delivery
Brightness
0.3
0.2
0.1
0
0.1
0.2
0.3
0.4
0.5
0.6
Lateral Distance (mm)

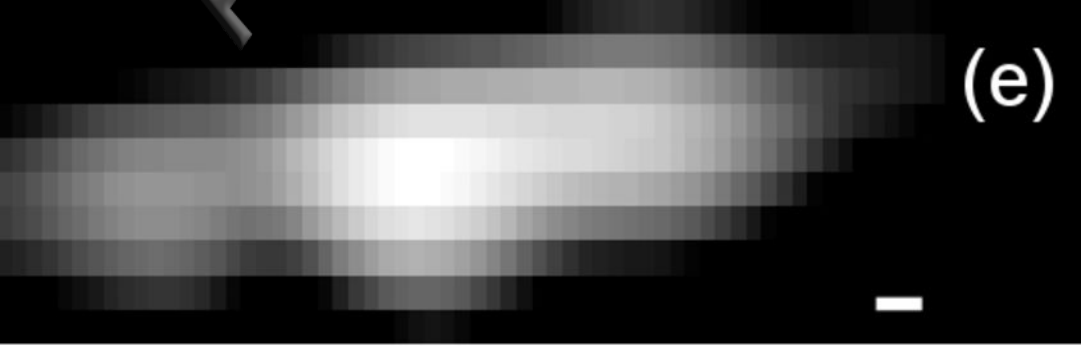
(e)

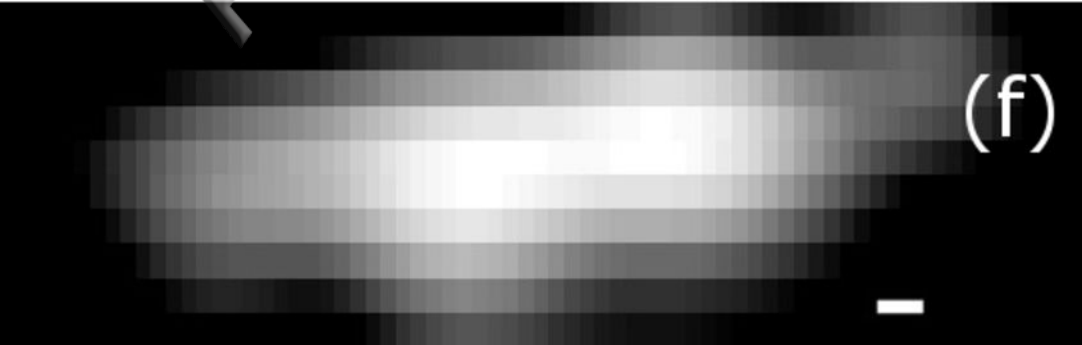
(f)